Design Considerations for a Space-Variant Visual Sensor with Complex-Logarithmic Geometry

Alan S. Rojer *Eric L. Schwartz*

Brain Research Laboratory
New York University Medical Center

Courant Institute of Mathematical Sciences
Department of Computer Science
New York University

Abstract

Human vision is both active and space-variant. Recent interest in exploiting these characteristics in machine vision naturally focuses attention on the design parameters of a space-variant sensor. We consider space-variant sensor design based on the conformal mapping of the half disk, $w = \log(z+a)$, with real $a>0$, which characterizes the anatomical structure of the primate and human visual systems. There are three relevant parameters: the "circumferential index" κ, which we define as the number of pixels around the periphery of the sensor, the "visual field radius" R (of the half-disk to be mapped), and the "map parameter" a from above, which displaces the logarithm's singularity at the origin out of the domain of the mapping. We show that the log sensor requires $\mathbf{O}(\kappa^2 \log(R/a))$ pixels. The pixel width in the fovea (foveal resolution) L_{fov} is proportional to a/κ. If we accept a fixed circumferential index (constant κ), the space complexity of the log sensor with respect to foveal resolution goes as $\mathbf{O}(-\log L_{\text{fov}})$. By contrast, a uniform-resolution sensor has a space complexity that goes as $\mathbf{O}(L_{\text{fov}}^{-2})$. Similarly, when the space complexity of the sensor is considered with respect to the field size with a fixed foveal resolution, we find that the space complexity goes as $\mathbf{O}(\log R)$, while for the uniform-resolution sensor, the space resolution goes as $\mathbf{O}(R^2)$. Using this analysis, it is possible to directly compare the space complexity of different sensor designs in the complex logarithmic family. In particular, we can obtain rough estimates of the parameters necessary to duplicate the field width/resolution performance of the human visual system.

Introduction

Human vision is both active and space-variant. Recent interest in exploiting these characteristics for machine vision naturally focuses attention on the design parameters of a space variant sensor. In the case of conventional space-invariant (or uniform-resolution) sensors, the number of pixels in the sensor provides a single number which characterizes space complexity. Given the number of pixels in a uniform sensor, the ratio of visual field width and sensor resolution is fully determined. Thus, it is a simple matter to compare conventional sensors. In contrast, the space complexity of space-variant sensors depends on the "architecture" of the sensor, with potentially enormous variation, which is beyond the scope of this paper. We focus our attention on a particular space-variant architecture, the conformal map associated with the complex logarithm, which characterizes a prominent part of the anatomical structure of the primate and human visual systems.

The complex-log mapping provides an accepted model of the mapping from retina to primary visual cortex in primates at both the local (hypercolumn) and global (retinotopic representation) scales [1-3]. Traditionally, researchers in computer vision have found motivation in small-scale (cellular) properties of biological vision: the application of the $\nabla^2 G$ operator for edge enhancement is one example [4]. The complex-log retinotopic representation is a striking example of the large-scale architecture of biological vision; for that reason alone it merits study as a potential architecture for computer vision.

The complex-log mapping of scenes also has favorable computational properties. It embodies a useful isomorphism between multiplication in its domain and addition in its range. This is especially interesting when a two-dimensional scene is considered to be defined with respect to a complex argument; then complex multiplication of the argument is equivalent to scaling of the scene (by the modulus of the multiplier) and rotation of the scene around the origin (by the argument of the multiplier). In the range of the log mapping, complex multiplication becomes addition, so the mapped image of the scene is shifted horizontally in proportion to the log of the scale change, and vertically in proportion to the angle of rotation. This isomorphism has been exploited for efficient implementation of computer graphic and image processing operations [5].

Models of the perceptual equivalence of scaled and rotated objects have also utilized the complex log mapping [1]. The problem of position, scale and rotation-independent template matching for images has been addressed by the use of Fourier-Mellin transforms [6,7]. To create a position-, scale- and rotation-independent template for an object, the magnitude of the Fourier transform of the object is first computed. This is invariant to shifts in position of the object. The complex-log mapping converts changes of scale and rotation (which are preserved in the magnitude of the original Fourier transform) to shifts in the range of the log mapping. A second Fourier transform magnitude (on the log scene) standardizes with respect to the shifts in the log scene, producing a template (for correlation) which is independent of the scale, position and rotation of the original object. The combination of log-mapping and Fourier transform is equivalent to the Mellin transform [8].

Other useful properties of the log-mapping have been discovered with regard to computations in a moving visual field. Determination of time-to-collision and depth-from-motion for a moving camera in a stationary world has been considered in [9-11]. It is readily apparent that when the camera is moving in a stationary world, the optical flow of the scene is purely radial. In the log-mapped image, this corresponds to pure horizontal flow. Deviations

from this flow, which indicate field objects with independent motion, can be determined by simple techniques which identify a vertical component of optical flow [10, 12].

Advances in VLSI technology have made the construction of a logarithmic sensor a possibility; for example, a CCD sensor which utilizes a logarithmic periphery and a uniform fovea has been described [13]. Thus, the goal of this paper is to elucidate the design parameters which relate external criteria of field width and resolution to internal geometry and space complexity (pixel count). An important corollary is the quantitative demonstration of the highly favorable performance of the log sensor with regard to the field-width/resolution trade-off. We will illustrate the complex-log mapping as a mathematical entity and as an image warp. After a brief discussion of the space complexity of a conventional uniform-resolution sensor, the space complexity of a log sensor will be calculated. We will examine various methods to increase resolution and field width. Quantitative comparisons of log sensors with conventional sensors will be presented. Finally, we will examine the dependence of a quality factor (the ratio of field width to foveal resolution) on the design parameters of the log sensor.

Complex Logarithm: Conformal Mapping and Image Warping

We will consider a space-variant sensor in which the mapping from "retinal" coodinates to "cortical" coordinates is given by the complex log transformation

$$w = \log(z+a),$$

with real $a>0$. (A spatial scale constant relating the dimensions of thge w plane to the z plane has been implicitly set to unity). More explicitly, we may write $w = u+iv$, with

$$u = \log|z+a|,$$

$$v = \arg(z+a).$$

In contrast to recent related work [14, 15] which uses the mapping $\log z$ ($a = 0$ in our notation), with a constant-resolution patch for the singularity at the origin, we use the mapping $\log(z+a)$, with real $a>0$. We select the latter mapping for sensor design since it is a better fit to biological data [12] and since it removes the singularity of the log mapping at the origin for the cost of managing a discontinuity on the vertical meridian (midline).

An example of the mapping $\log(z+a)$ is shown in Figure 1. The key features of the mapping are as follows. In the fovea ($|z|<a$), the mapping is nearly linear. This can be seen from the Taylor series expansion of the mapping $f(z) = \log(z+a)$ in the region of the origin:

$$f(z) \approx f(0)+f'(0)z.$$

But $f(0) = \log a$, and $f'(0) = a^{-1}$. The mapping is just a translation by $\log a$ and a scaling by the factor a^{-1}. Outside the fovea, the map rapidly approaches the pure log. In this case, the familiar properties of the complex log mapping hold: circles in the domain are mapped to vertical lines in the range, and rays in the domain are mapped to horizontal lines in the range. Locally, the mapping near an arbitrary position z_0 looks like scaling inversely with the magnitude $|z_0|$, with a rotation of $-\arg z_0$.

The complex log mapping may be illustrated as a warping of a conventional scene (Figure 2). We associate with each pixel W from the range (i.e. the log-mapped scene, Figure 2b) a set of domain pixels $f^{-1}(W)$ (from the original scene, Figure 2a) which map into W under the log map. For simplicity, we ignore the finite area of a domain pixel Z, representing the pixel by a point $\chi_Z \in Z$. Formally,

$$f^{-1}(W) = \{Z \mid \log(\chi_Z+a) \in W\}.$$

Now we compute the brightness of a range pixel W by averaging over the brightnesses of pixels $Z \in f^{-1}(W)$. A conventional image is shown in Figure 2a; a log-mapping of the image is shown in Figure 2b. Note that the mapping depends very strongly on the location of the origin in the domain (denoted the fixation point). The inverse-mapping of the log scene to uniform coordinates is shown in Figure 2c; note that substantial resolution has been lost in extrafoveal regions, while the foveal reconstruction shows little loss of resolution. The inverse image of individual pixels from the periphery of the log-map can be clearly seen in the inverse-mapped scene. These regions indicate the actual size and orientation of sensor pixels in a sensor which utilizes the complex-log geometry.

Space Complexity of a Uniform-Resolution Sensor

We will quickly summarize the space complexity of a uniform-resolution sensor to establish notation that will facilitate comparison with the log sensor. We will consider a circular visual field, for consistency with the analysis of the log sensor below. Let the radius of the visual field be R, and let the *radial index* ρ be defined as the number of pixels along a radial traverse of the visual field (we ignore the slight variation of ρ for different radii due to pixel quantization). Then the (uniform) resolution L_{unif} is given by

$$L_{\text{unif}} = \frac{R}{\rho}.$$

The number of pixels required for the full circular field is given by

$$N_{\text{unif}} = \pi\rho^2 = \pi\left(\frac{R}{L_{\text{unif}}}\right)^2 \tag{1}$$

Pixels in the Log Mapping

We assume pixels in the range are square and uniformly sized (see Figure 2). We also assume a circular visual field to simplify the analysis. Let the radius of the visual field be given by R. Define the "circumferential index" κ as the number of pixels around the disk comprising the visual field of the sensor. We have already introduced the geometric "map parameter" a which eliminates the discontinuity in the log map at $z = 0$.

We will approximate with a grid of pixels the mapping

$$w = \log(z+a), \tag{2}$$

restricting consideration to the mapping of the right half-disk of radius R, $|z| \le R, -\frac{\pi}{2} < \arg z \le \frac{\pi}{2}$. The other half-disk receives nearly symmetrical treatment, using the map

$$\bar{w} = 2\log a - \log(-\bar{z}+a), \tag{3}$$

where $\bar{w}$ is the complex conjugate of w, and $-\bar{w}$ is equivalent to a reflection around the imaginary axis. The composite mapping of the two half-disks via (2) and (3) results in the characteristic "butterfly" shaped log scene of Figure 2b.

The range of the mapping of the right half-disk is contained in the strip bounded by

$$-\frac{\pi}{2} < v \le \frac{\pi}{2},$$

$$\log a \le u \le \log(R+a).$$

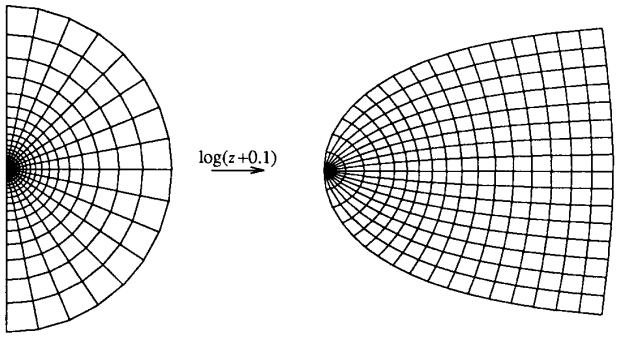

Figure 1 The conformal mapping of the unit half-disk by $\log(z+a)$, shown here with $a=0.1$. The vertical meridian in the domain is mapped to the curved boundary at left in the range, while the unit half-circle is mapped to the (nearly vertical) right boundary of the range. Of particular interest is the dramatic expansion of the "foveal" region, which is barely discernable in the domain. In the periphery, the mapping is quite similar to the "pure" log with $a=0$, with domain rays mapped to nearly horizontal lines, and circles mapped to nearly vertical lines. In the fovea, however, the map is nearly linear. This is apparent for the innermost ring of (triangular) pixels, which is almost unchanged in shape in the range, although it has been greatly expanded (by a factor of $1/a$).

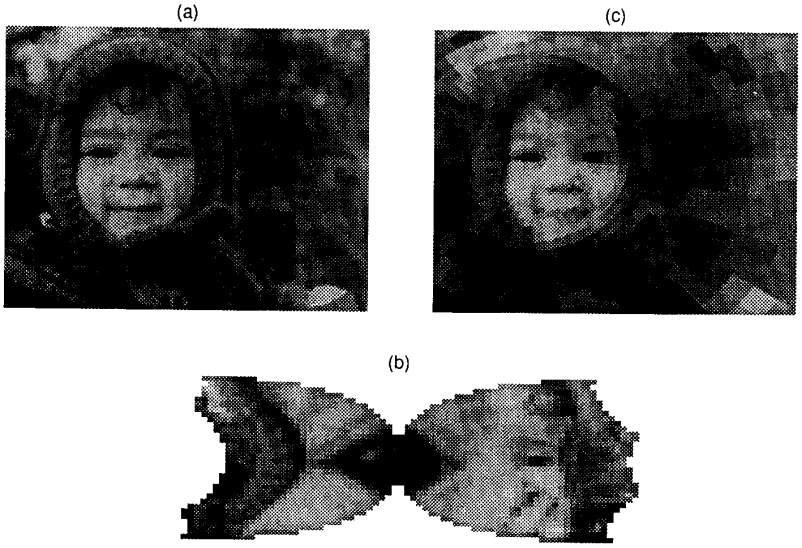

Figure 2 The log map of an image and its inverse (counterclockwise from top left). **(a)** The source image, 472×508 pixels. **(b)** The log map of the image, map parameters $a = 10.19$, $\kappa = 64$, $R = 512$; image size 32×80 pixels. **(c)** The inverse mapping of the log image. This is an approximation to the original image using only the information in the log image.

The circumferential resolution κ determines the pixel size in the range; the width l of a range pixel will be given by

$$l = \frac{2\pi}{\kappa}. \tag{4}$$

Since the pixels are uniform and square in the range, we can immediately determine the number of pixels along the image of the horizontal meridian in the range, which determines the width (in pixels) of the range. The length of the image of the horizontal meridian is twice $\log(R+a) - \log a$. Note, however, that $R \gg a$, so in effect, the horizontal meridian image has length $2\log(R/a)$ Using the pixel width in the domain from (4), the number of pixels n along the image of the meridian is given by

$$n = \frac{2\log(R/a)}{l} = \frac{\kappa}{\pi}\log\frac{R}{a}. \tag{5}$$

This bounds the width (in pixels) of the log-mapped scene. The height of the log-mapped scene is simply the number of pixels for the interval $[-\pi/2, \pi/2]$; i.e. $\kappa/2$. Multiplying height and width of the log scene, we determine that the total number of pixels in the log map of the disk $N_{\log}$ is bounded by

$$N_{\log} \leq \frac{\kappa}{2}n = \frac{1}{2\pi}\kappa^2\log\frac{R}{a} \tag{6}$$

The resolution of a pixel is determined by its size in the domain. For sufficently small pixel size, the "magnification" $m(Z)$ of a domain pixel Z is roughly constant over the pixel, and it is given by the magnitude of the derivative of the log map

$$m(Z) \approx |w'(\chi_Z)| = \frac{1}{|\chi_Z + a|}, \tag{7}$$

evaluated at some point $\chi_Z \in Z$.

From Eq. (7), it is apparent that, in the fovea ($|\chi_Z| \approx 0$), we have a magnification $m_{\text{fovea}} = a^{-1}$. Working back from the range pixel size l (4), we determine that the foveal domain pizel size L_{fov} is given by

$$L_{\text{fov}} = \frac{l}{m_{\text{fovea}}} = 2\pi\frac{a}{\kappa}. \tag{8}$$

For extrafoveal pixels ($|\chi_Z| \gg a$), observe

$$L(Z) = \frac{l}{m(Z)} \approx 2\pi\frac{|\chi_Z|}{\kappa}. \tag{9}$$

We observe that the foveal resolution depends on both parameters a and κ. In practice, this implies two routes to increasing foveal resolution: changing the geometry of the log map (decreasing a), and increasing the circumferential index κ. We will consider these approaches separately; we note here that decreasing a does not affect the extrafoveal resolution, while increasing κ increases the resolution throughout the map.

Increasing Foveal Resolution by Geometry

For a given log sensor, characterized by parameters R, κ, and a, we have noted two routes to increase the foveal resolution. In this section, we will consider the effect of changing sensor geometry. Eq. (8) indicates the linear relationship between the map parameter a and the foveal pixel width L_{fov}. In geometric terms, decreasing a has the effect of lengthening the bullet-like "nose" of the log map (Figure 3).

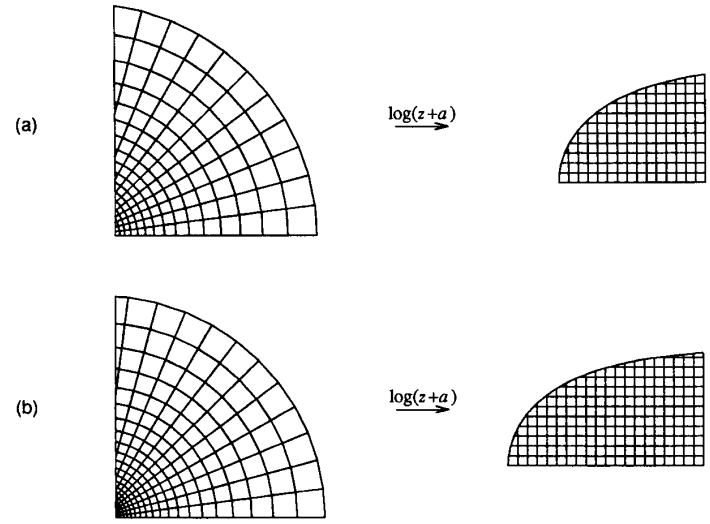

Figure 3 Foveal pixel size L_{fov} is proportional to the map parameter a. The space complexity $N_{\log}$ of the sensor with fixed circumferential index κ (fixed angular resolution $2\pi/\kappa$) goes as $N_{\log} = O(-\log L_{\text{fov}})$. **(a)** One quadrant of a sensor utilizing complex-logarithmic geometry; $a = 0.150$, $R = 1.00$, $\kappa = 48$. **(b)** Increasing the resolution of the sensor by halving a; $a = 0.075$, $R = 1.00$, $\kappa = 48$. L_{fov} has also been halved (doubled resolution).

We next determine the space complexity (number of pixels) of the sensor as a function of the foveal resolution, holding κ and R constant. Rearranging Eq. (8) for a as a function of foveal resolution, obtain

$$a = \frac{1}{2\pi}\kappa L_{\text{fov}}.$$

Substituting into Eq. (6) for the number of pixels in the sensor, holding R and κ constant, obtain

$$N_{\log}[a]_{R,\,\kappa=\text{const}} = \frac{1}{2\pi}\kappa^2 \log\frac{\pi R}{\kappa L_{\text{fov}}}$$

$$= \mathbf{O}(-\log L_{\text{fov}}). \tag{10}$$

The number of pixels required for a log sensor increases logarithmically with the maximum resolution of the sensor when increases in resolution are obtained by changing the map parameter a. In contrast, we can determine from (1) that the space complexity of the uniform-resolution sensor with constant R goes with the inverse square of the foveal resolution.

For a simple comparison, consider a unit radius visual field ($R = 1$) with a foveal resolution of $L = 1/256$. With a uniform-resolution sensor, $L_{\text{unif}} = 1/256$, and we require (from Eq. (1)) approximately 206,000 pixels. Now consider a log sensor with $\kappa = 64$ and $L_{\text{fov}} = 1/256$. From (8), $a \approx 0.040$, and 7 reveals $N_{\log} \approx 2100$.

Now let the foveal resolution be doubled to $L = 1/512$. Then a becomes 0.02, and $N_{\log} \approx 2550$. The uniform-resolution sensor requires about 823,000 pixels, an increase of 300%, while the log sensor requires an increase of only 21%.

Increasing Foveal Resolution by Subdivision

We obtained an increase in foveal resolution by changing the geometry of the log map in the previous section. Here we will increase the foveal resolution by subdividing pixels. More precisely, we will increase the circumferential index κ, increasing the number of pixels around each concentric ring in the sensor as well as the total number of rings in the sensor (Figure 4).

For any particular foveal resolution L_{fov} and map parameter a we will obtain (by rearrangement of Eq. (8))

$$\kappa \propto \frac{a}{L_{\text{fov}}}.$$

Substituting into (Eq. (6)) for the number of pixels in the log sensor and holding a and R constant, we obtain

$$N_{\log}[\kappa]_{R,\,a=\text{const}} = \frac{1}{\pi}\left[\frac{a}{L_{\text{fov}}}\right]^2 \log\frac{R}{a}$$

$$= \mathbf{O}(L_{\text{fov}}^{-2}).$$

This is the same space complexity as the uniform-resolution sensor.

Increasing Field Width by Expansion

Another important characteristic of a sensor is the radius R of the visual field to which it is responsive. In the case of a uniform-resolution sensor, if we keep L_{fov} constant while changing R, we find (Eq. (1))

$$N_{\text{unif}} = \mathbf{O}(R^2).$$

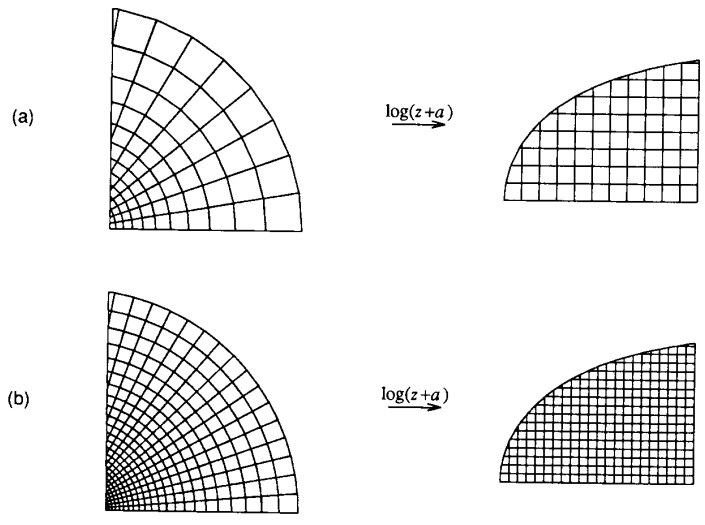

Figure 4 Foveal pixel size L_{fov} is inversely proportional to the circumferential index κ. The space complexity $N_{\log}$ of the sensor with fixed map parameter a goes as $N_{\log} = \mathbf{O}(\kappa^2)$. (**a**) One quadrant of a sensor utilizing complex-logarithmic geometry; $a = 0.150, R = 1.00, \kappa = 36$. (**b**) Increasing the resolution of the sensor by increasing κ; $a = 0.150, R = 1.00, \kappa = 72$. Like the uniform-resolution sensor, doubling foveal resolution by increasing κ results in squaring the space complexity $N_{\log}$. In contrast to changes in foveal resolution via the map parameter a, increases in κ also affect the peripheral resolution; peripheral pixel size L_{peri} is inversely proportional to κ.

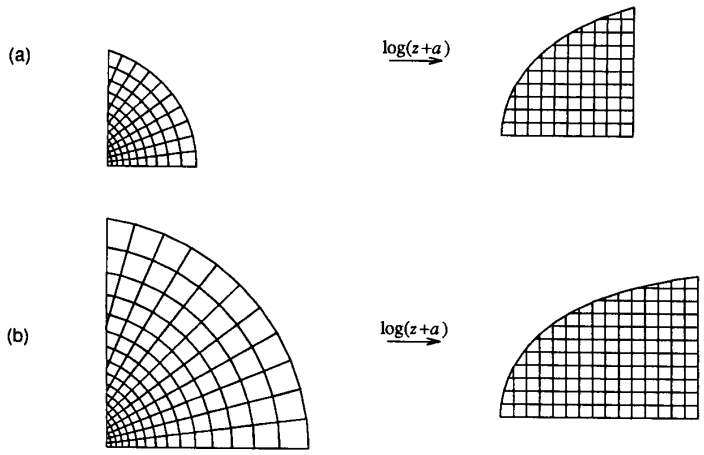

Figure 5 Changing the field width R of the sensor while keeping the circumferential index κ fixed affects the space complexity $N_{\log}$ as $O(\log R)$. **(a)** The cortical representation and sensor geometry induced when $a = 0.150, R = 0.50, \kappa = 48$. **(b)** Increasing the field width of the sensor by increasing R; $a = 0.150, R = 1.00, \kappa = 48$. Note also that the peripheral pixel size L_{peri} has increased (a decrease in spatial resolution, but constant angular resolution) with the increase in R since $L_{\text{peri}} \propto R$. To keep L_{peri} constant while increasing R requires changing κ and a, with a concordant impact on the space complexity $N_{\log} = O(R^2)$.

There are two possibilities for increasing the field width with a log sensor, depending on whether we fix the extrafoveal resolution or not. In the simpler case, we hold the circumferential index κ and the foveal resolution L_{fov} constant (Figure 5). Then a is also fixed, via (8). Applying Eq. (6), and holding L_{fov} and κ constant, we find

$$\begin{aligned} N_{\log}[R]_{\kappa, L_{\text{fov}}=\text{const}} &= \frac{1}{2\pi}\kappa^2 \log \frac{R}{a} \\ &= \frac{1}{2\pi}\kappa^2 \log \frac{\pi R}{\kappa L_{\text{fov}}} \\ &= O(\log R). \end{aligned}$$

At the cost of increased pixel size in the periphery, we obtain a space complexity which is logarithmic in the field width. In comparison, the uniform-resolution sensor under similar conditions has a space complexity which goes as the square of field width.

In the last analysis, we accepted a decreased peripheral resolution as a conseqence of increased field size. This comes about because we have fixed the circumferential index κ while R has increased; thus the extrafoveal pixel size, which is proportional to R/κ, has increased (hence the resolution has decreased). Alternatively stated, we have kept our peripheral *angular* resolution constant but, because the peripheral radius is larger, the *spatial* resolution has decreased.

If we wish to preserve spatial resolution in the periphery we have to increase κ as the field size increases. In this case, we have the same consequences as when we increased foveal resolution by subdivision: the space complexity goes as $O(\kappa^2)$, and, since κ will be proportional to R to keep peripheral resolution constant, the sensor space complexity will go as $O(R^2)$, which is the same as the uniform-resolution sensor.

Log Sensor and Uniform-Resolution Sensor: a Comparison

To illustrate the quantitative results obtained above, we will consider some detailed comparisons between conventional and log sensors for biological and VSLI systems. Consider first design of a space-variant VLSI sensor utilizing the complex-log geometry. Assume design criteria as follows. Let the diameter of the sensor $2R = 20\text{mm}$. Let the size of the smallest pixel in the sensor $L_{\text{fov}} = 20\mu$. Fixing $\kappa = 64$, determine from (8)

$$a = \frac{1}{2\pi}\kappa L_{\text{fov}} \simeq 200\mu.$$

For the total number of pixels, use (6) to obtain

$$N_{\log} \leq \frac{1}{2\pi}\kappa^2 \log \frac{R}{a} \simeq 2550.$$

A circular, uniform-resolution sensor with $L = 20\mu$ and $R = 10\text{mm}$ will have radial index $\rho = R/L_{\text{fov}} = 500$. Assuming a circular field, the uniform sensor would contain nearly 800,000 pixels.

Consider next a model of the primate eye as a log sensor. An empirical fit to the retina-to-cortical mapping has been derived from published data [3, 16] which is roughly

$$w = b \log (z+a),$$

with w in mm of cortex, a in retinal degrees of visual field, and scaling constant $b \simeq 5$ mm/degree. This implies a cortical magnification factor

$$m = \frac{b}{|z+a|}.$$

When $z = 0$ (in the fovea), obtain $m = b/a$. In the fovea, $m \simeq 15$ mm/degree.

The units of magnification factor (mm/degree) are not strictly consistent with the magnitude of the derivative of the complex logarithm. Note that the primary visual cortex in the macaque is about 20 mm across, corresponding to π radians vertically in the range of the logarithm. We thus introduce a cortical scale factor $c = 20/\pi$ mm/radian.

Next we introduce a sampling parameter s. To obtain a particular resolution L_{fov}, we must sample the scene with at least twice the frequency implied by the desired resolution; formally $s \geq 2$. The retinal pixel size in the fovea will be given by L_{fov}/s. Now we can express the size l of a foveal "pixel" at the cortical surface,

$$l = m\frac{L_{fov}}{s} = \frac{2\pi}{\kappa}c.$$

The second expression is the magnification of a retinal pixel; the third expression is the physical size of a cortical pixel. Note the equation has units of mm. The foveal resolution L_{fov} has been determined by psychophysical investigation to be roughly 1 minute of arc. The only unknown is the circumferential index κ. Rearranging, we obtain

$$\kappa = \frac{2\pi cs}{mL_{fov}}.$$

Setting the sampling parameter $s = 3$ (a conservative value; $s = 2$ is theoretically sufficient), and substituting, obtain $\kappa \approx 432$. The visual field ($2R$) of the primate eye is about 140 degrees vertically, and slightly larger than this (roughly 200 degrees) horizontally. To simplify this comparison, we arbitrarily set ($2R$) at 150 degrees, noting that the following analysis is very insensitive to the limits of the far periphery, due to the enormous compression of visual field there. From (6), the required number of pixels for a sensor to approximate the eye can be estimated; we obtain $N_{log} \approx 164{,}000$. This estimate is consistent with the number of fibers in the optic tract (about 1,000,000), since we have not accounted for multiple color channels, duplication for on-center and off-center retinal ganglia, and non-cortical afferents. Thus, a sensor in the range of $N_{log} \approx 10^5$ is comparable to the (monocular, monochromatic) human retino-cortical system.

To achieve comparable resolution and field width in a uniform sensor would require $\pi(sR/L_{fov})^2$ pixels, or nearly 600,000,000 pixels. Estimates of "pixels" in the eye are necessarily crude, but the order-of-magnitude estimate presented here makes clear the prohibitive cost of reproducing the field-width/resolution performance of the primate eye with a uniform sensor.

F/R Quality

We can introduce a simple figure of merit for a sensor which accounts for field width $2R$ and foveal resolution L_{fov}. Let

$$Q = \frac{R}{L_{fov}}$$

be termed the *field-width/resolution quality*, or simply *F/R quality* of a sensor. In the case of a uniform-resolution sensor, we use Eq. (1) to obtain

$$Q_{unif} = \rho, \tag{11}$$

where ρ has been previously defined as the number of pixels along a radial traverse of the sensor. For a log sensor, the F/R quality is more complex; using Eq. (8) we find

$$Q_{log} = \frac{\kappa R}{a}, \tag{12}$$

where κ is the circumferential index and a is the geometric map parameter. This expression illustrates the various tradeoffs that are possible with a log sensor. For example, sensors of equal F/R quality can trade-off the circumferential index against the geometric map parameter without sacrificing field width. This is relevant in the light of Eq. (6), which gives the space complexity of the log sensor as

$$N_{log} = \mathbf{O}(\kappa^2 \log \frac{R}{a}).$$

In the event that κ may be supposed fixed (i.e. the sensor will have a fixed angular resolution), we find that the number of pixels goes as $\mathbf{O}(\log R/a)$, which is an outstanding property of the sensor.

A general measure of the utility of a sensor geometry in the light of F/R quality is the functional dependence of Q on the number of pixels in the image. A function which grows rapidly as the number of pixels is increased suggests a very efficient sensor; i.e. one which is turning additional pixels into additional quality at a very good rate. For the uniform-resolution sensor, since $\rho \propto \sqrt{N_{unif}}$, we observe

$$Q_{unif}(N_{unif}) = \mathbf{O}(\sqrt{N_{unif}}).$$

For the log sensor, if we hold κ constant (i.e. accept a fixed angular resolution) then we obtain

$$Q_{log}(N_{log}) = \mathbf{O}\left[\frac{R}{a}\right] = \mathbf{O}(\exp N_{log}).$$

This is a striking characterization of the utility of the log geometry for sensor design with respect to F/R quality.

Conclusion

The log sensor has been found to have very favorable space complexity under the restriction of fixed angular resolution. The good results for asymptotic complexity are borne out in practical situations; in the simulation presented above, a log sensor matched the F/R quality of a uniform-resolution sensor with about 1/50 the pixels. Previous workers have emphasized geometric properties of the log map in hypotheses for its use in primate vision and proposals as a possible architecture for machine vision. The results presented here indicate that the favorable space complexity of the sensor with respect to F/R quality is another compelling reason for application of the log map in vision.

We conclude by indicating some of the challenges which complicate the use of the log sensor. The technical problems of fabricating a sensor with space-variant elements have apparently been solved using CCD technology [13]. The problem of "attention" is foremost in the application of a log sensor: the vision system must be able to determine where to point its high-resolution fovea, and it must be physically capable of quick, accurate positioning of the sensor. The problems of image understanding take on new forms with a space-variant sensor. Conventional processing of the log image (e.g. convolution with a fixed-size kernel) has unusual characteristics reminiscent of multiresolution architectures. The incorporation of data from multiple fixations to construct a world model is an interesting problem. The necessities of attention introduce a new strategic component to object recognition algorithms; the fovea can be directed to positions which are expected to yield important information for recognition or disambiguation. Although many difficult problems must be confronted in the application of the log sensor geometry to machine vision, we are motivated by the example of biological vision, the useful geometric characteristics of the log-mapping, and the favorable field-width/resolution characteristics illustrated in this paper.

References

1. E. L. Schwartz, Spatial mapping in primate sensory projection: analytic structure and relevance to perception, *Biological Cybernetics 25*: 181-194 (1977).
2. D. Weinshall and E. L. Schwartz, A new method for measuring the visuotopic map function of striate cortex: validation with macaque data and possible extension to measurement of the human map, *Soc. Neuro. Abstr.* : 1291(1987).
3. E. L. Schwartz, A. Munsif and T. D. Albright, The topographic map of macaque V1 measured via 3D computer reconstruction of serial sections, numerical flattening of cortex, and conformal image modeling, *Investigative Opthalmol. Supplement* (in press).
4. D. Marr and E. Hildreth, Theory of edge detection, *Proc. R. Soc. Lond. B 207*: 187-217 (1980).
5. C. F. Weiman and G. Chaikin, Logarithmic spiral grids for image-processing and display, *Computer Graphics and Image Processing 11*: 197-226 (1979).
6. J. K. Brousil and D. R. Smith, A threshold-logic network for shape invariance, *IEEE Transactions on Computers EC-16*: 818-828 (1967).
7. D. Casasent and D. Psaltis, Position, rotation and scale-invariant optical correlation, *Applied Optics 15*: 1793-1799 (1976).
8. R. N. Bracewell, *The Fourier Transform and Its Applications*, McGraw Hill, 1978.
9. R. Jain, S. L. Bartlett and N. O'Brien, Motion stereo using ego-motion complex logarithmic mapping, *PAMI 3*: 356-369 (1987).
10. C. F. R. Weiman, 3-D sensing with polar exponential sensor arrays, *SPIE Conf. Digital and Optical Shape Representation and Pattern Recognition* (1988).
11. G. Sandini, F. Bosever, F. Bottino and A. Ceccherini, The use of an antropomorphic visual sensor for motion estimation and object tracking, *Proc. OSA Topical Meeting on Image Understanding and Machine Vision* (in press).
12. E. L. Schwartz, Computational anatomy and functional architecture of striate cortex: a spatial mapping approach to perceptual coding, *Vision Research 20*: 645-669 (1980).
13. J. Spiegel, F. Kreider, C. Claiys, I. Debusschere, G. Sandini, P. Dario, F. Fantini, P. Belluti and G. Soncini, A foveated retina-like sensor using CCD technology, in *Analog VLSI Implementations of Neural Networks*, C. Mead and M. Ismail (editors), Kluwer, Boston, 1989.
14. C. F. R. Weiman, Exponential sensor array geometry and simulation, *SPIE Conf. Digital and Optical Shape Representation and Pattern Recognition* (1988).
15. G. Sandini and P. Dario, Active vision based on space-variant sensing, *Fifth Int. Symp. on Robotics Research (ISSR)* (in press).
16. B. Dow, R. G. Vautin and R. Bauer, The mapping of visual space onto foveal striate cortex in the macaque monkey, *J. Neuroscience 5*: 890-902 (1985).